From: Victoria Bogdan Tejeda [mailto:vbogdantejeda@biologicaldiversity.org]
Sent: Tuesday, March 21, 2023 3:32 PM
To: CityClerk <CityClerk@longbeach.gov>
Subject: CBD Sources, 4.4

-EXTERNAL-

Attached:
The Impact of the BP Oil Spill
Yeck 2017
Xie 2008
Wu 2008

Victoria Bogdan Tejeda (*she/her*)
Staff Attorney, Climate Law Institute
Center for Biological Diversity
1212 Broadway, Suite 800
Oakland, CA 94612
Ph: 510.844.7103 ext. 303

TOURISM ECONOMICS

The Impact of the BP Oil Spill on Visitor Spending in Louisiana

Prepared for the Louisiana Office of Tourism

December 2010

TOURISM ECONOMICS

Overview

Tourism to Louisiana was unambiguously affected by the oil spill resulting from the explosion of the Deepwater Horizon oil rig in April, 2010. The threats from the oil spill, both real and perceived, to the gulf shoreline, waters, and seafood have impacted Louisiana tourism. Surveys of visitor perceptions conducted on behalf of the Louisiana Office of Tourism after the oil spill report a high rate of trip cancellations by leisure travelers. Travel surveys of actual visitors and tourism data confirm this for the second quarter of 2010. The descent of media, relief workers, and government officials has offset some of the lost spending from leisure travel in the near term. This report estimates past and prospective impacts on visitor spending resulting from the oil spill through the year 2013.

Summary results

- Lost visitor spending is expected to total $295 million through 2013
- This represents a decrease of 0.8% from the baseline forecast over the 2010-2013 period
- Leisure tourism is expected to experience a $691 million loss compared with the baseline forecast through 2013. This represents a cumulative 2.7% drop from pre-spill projections for leisure travel spending
- However, this is offset by an increase of 3.9% ($395 million) in business visitor spending resulting from the increase of media and company and government officials
- The effects on visitor spending are expected to persist into 2013 Q1 before returning to the baseline forecast

Louisiana Visitor Spending Loss

$ million, relative to baseline forecast

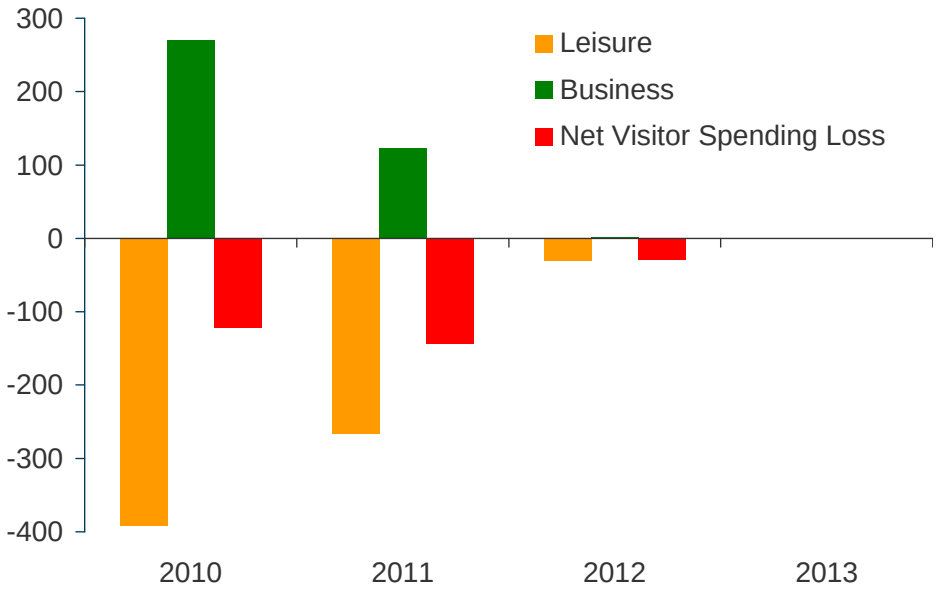

Source : Tourism Economics/Louisiana Office of Tourism

Louisiana Leisure Visitor Spending

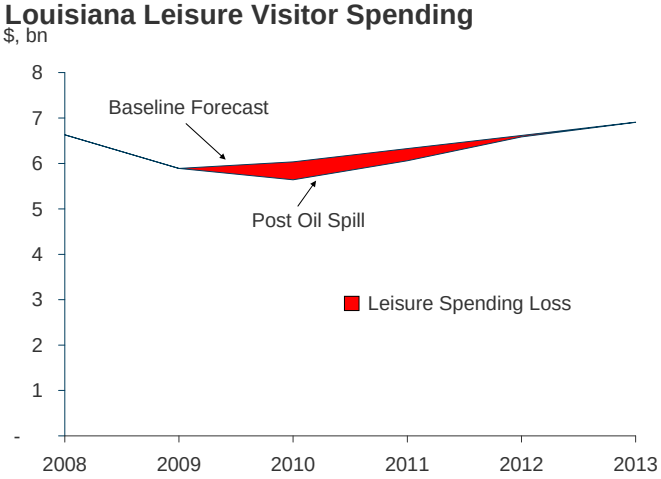

Source : Tourism Economics/Louisiana Office of Tourism

Louisiana Business Visitor Spending

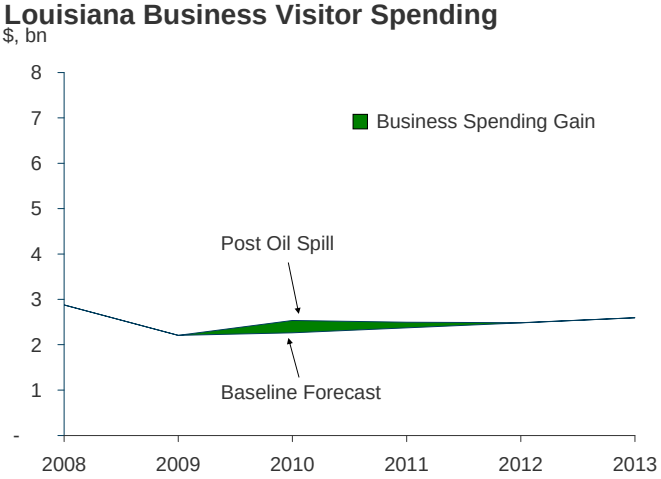

Source : Tourism Economics/Louisiana Office of Tourism

Louisiana Visitor Spending

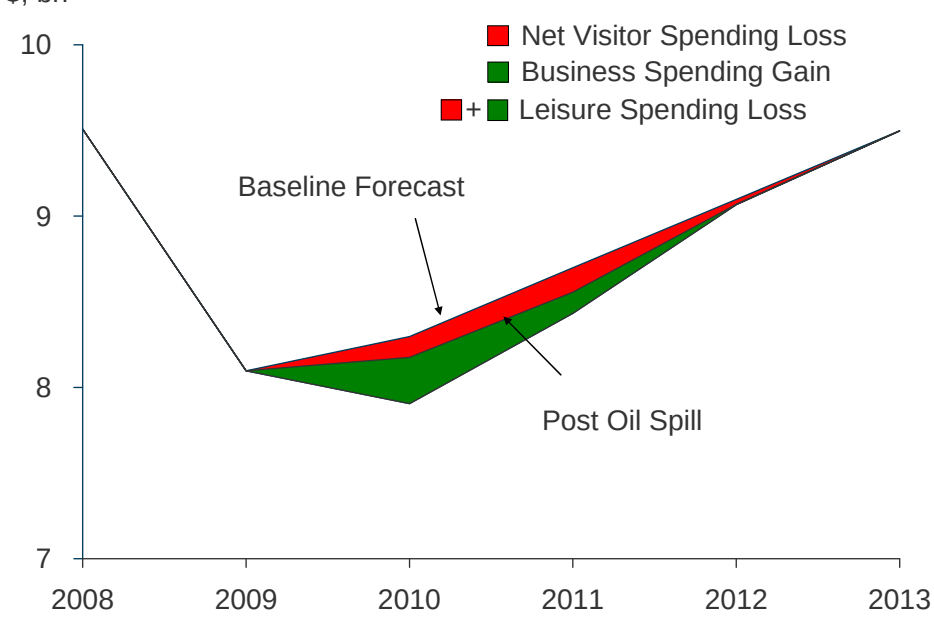

Source : Tourism Economics/Louisiana Office of Tourism

Louisiana Visitors Oil Spill Impact, million		2010	2011	2012
Baseline Forecast		24.2	24.7	25.3
	Business	6.3	6.4	6.6
	Leisure	17.9	18.3	18.7
Post Oil Spill		23.8	24.3	25.2
	Business	7.0	6.8	6.6
	Leisure	16.8	17.6	18.7
Lost Leisure Visitors		-1.1	-0.7	-0.1
% of Baseline Forecast		-4.5%	-2.9%	-0.3%
Offsetting Business Visitors		0.7	0.3	0.0
% of Baseline Forecast		3.0%	1.3%	0.0%
Net Visitor Loss		-0.4	-0.4	-0.1
% of Baseline Forecast		-1.5%	-1.6%	-0.2%
Cumulative Visitors Lost		-0.4	-0.8	-0.8
% of Baseline Forecast		-1.5%	-1.5%	-1.1%

Louisiana Visitor Expenditure Oil Spill Impact, $ million		2010	2011	2012	2013
Baseline Forecast		8,297.6	8,698.8	9,097.6	9,498.6
	Business	2,263.4	2,373.3	2,483.4	2,593.2
	Leisure	6,034.2	6,325.5	6,614.2	6,905.4
Post Oil Spill		8,175.7	8,555.4	9,068.5	9,497.7
	Business	2,534.1	2,496.1	2,485.2	2,593.2
	Leisure	5,641.6	6,059.3	6,583.3	6,904.5
Lost Leisure Spending		-392.6	-266.2	-30.8	-0.9
% of Baseline Forecast		-4.7%	-3.1%	-0.3%	0.0%
Offsetting Business Spending		270.7	122.8	1.8	0.0
% of Baseline Forecast		3.3%	1.4%	0.0%	0.0%
Lost Visitor Spending		-121.9	-143.4	-29.1	-0.9
% of Baseline Forecast		-1.5%	-1.6%	-0.3%	0.0%
Cumulative Lost Revenue		-121.9	-265.3	-294.4	-295.3
% of Baseline Forecast		-1.5%	-1.6%	-1.1%	-0.8%

Oil Spill Impacts on Visitor Spending

Just prior to the explosion of the Deepwater Horizon oil rig, the "Louisiana Tourism Forecast: 2009-2013" was published by the University of New Orleans Hospitality Research Center and Louisiana State University Division of Economic Development on behalf of the Louisiana Department of Culture, Recreation and Tourism. This forecast provides our analysis with a useful baseline against which to assess the impacts of the oil spill on tourism spending. That is, the baseline forecast provides us with a model of what would have been absent the oil spill.

Our analysis quantifies the initial impacts on tourism volumes and spending using available data for the period since the explosion of the Deepwater Horizon. We then model continuing effects on visitor volume using inputs from surveys of visitor perception and intentions to travel to Louisiana collected after the oil spill as well as the baseline forecast. The visitor spending impact is then the resulting difference between the baseline spending forecast and the post oil spill spending forecast until the two forecasts converge.

While the model as presented above is conceptually simple, travelers are not a homogenous group. Therefore, differences in types of travelers must be considered. The model estimates the impacts on business and leisure visitors separately. Leisure visitors are more likely to be negatively affected by the oil spill. The most obvious segment affected would be the 10% of Louisiana visitors in 2009 reporting trip activities including outdoor recreation/fishing and usage of beaches.

Another important factor is seasonality. We developed our model on a quarterly basis to account for the differing levels of tourism activity during the year and to more accurately account for changing perception over time. Given an impact in absolute terms, the relative effect of that impact will differ depending on the timing of the impact within the year. Historically, the peak travel season in Louisiana has been the 1st and 2nd quarters, with the peak typically in the 2nd quarter. A detailed description of the methodology used to develop the quarterly model appears in the final section of this report.

Initial Impact

Our period of analysis begins in the second quarter of 2010, the quarter in which the explosion of the Deepwater Horizon occurred. Data were compiled from a number of sources to estimate the initial impact on tourism. These data include industry data covering

- hotel performance;
- air enplanements at Louisiana airports;
- gross receipts for hotels;
- gross receipts for car rental companies;
- gaming revenue from the Louisiana Department of Revenue;
- fishing licenses sold and revenue from the Louisiana Department of Wildlife and Fisheries;

- Louisiana Welcome Center visitors from the Louisiana Office of Tourism; and
- National survey results of prospective visitors.

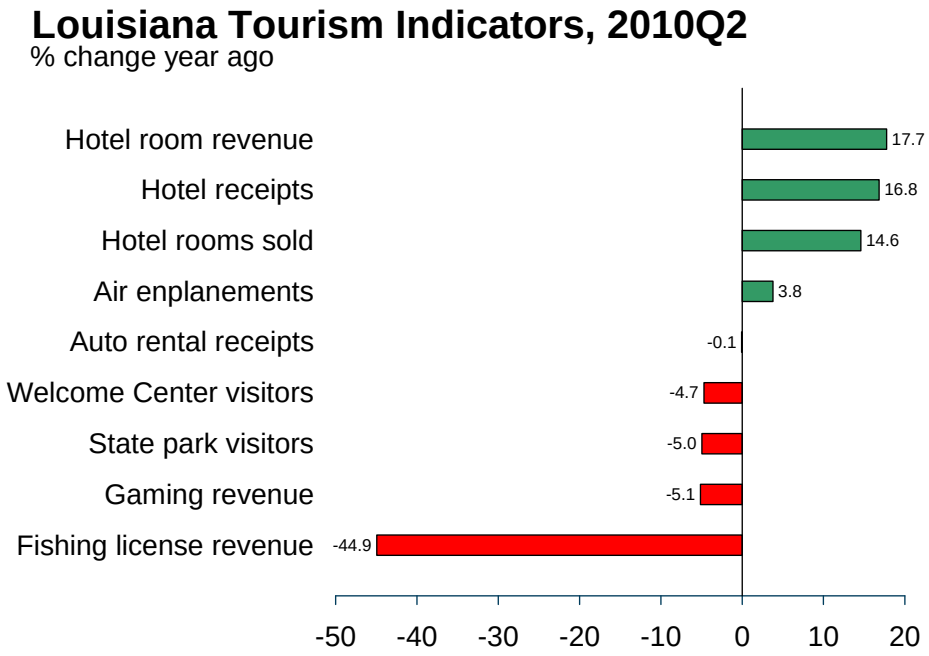

Source : STR, Louisiana Office of Tourism, Louisiana Department of Revenue, Louisiana Department of Wildlife & Fisheries

There are two competing dynamics apparent in the data. Hotels fared very well at the beginning of this crisis. The number of hotel rooms sold in the second quarter was up nearly 15% over 2009. However, fewer visitors passed through Louisiana welcome centers and visits to state parks also declined. Both declined by approximately 5% and are indicative of leisure travel volumes. Thus, the increase in hotel room demand can be partially explained by an increase in business travel (with the other part being an increase in the average length of stay). This is expected in the current context given the presence of activity related to the oil spill and cleanup efforts.

Additionally, MDRG has conducted multiple surveys of leisure travelers on behalf of the Louisiana Office of Tourism. The national surveys, conducted in May and August and regional surveys, conducted in June and September, identify those leisure travelers who had plans to visit Louisiana and cancelled their plans after the oil spill.

Visitors in the national survey were more likely to have cancelled or postponed trips after the oil spill. In May 2010, 26% of respondents who had planned trips to Louisiana prior to the oil spill had either cancelled or postponed their trips after the oil spill. Regional travelers had cancelled or postponed only 17% of planned trips to Louisiana in June, but that number had improved to 13% by September.

The hypothesis that business travel has otherwise bolstered the loss of leisure travelers is confirmed in 2nd quarter travel survey data released by TNS. Their survey results show declining leisure travel in the face of a strong increase in business visitation.

Cancelled/postponed trips after oil spill

% of respondents with plans to visit Louisiana prior to oil spill

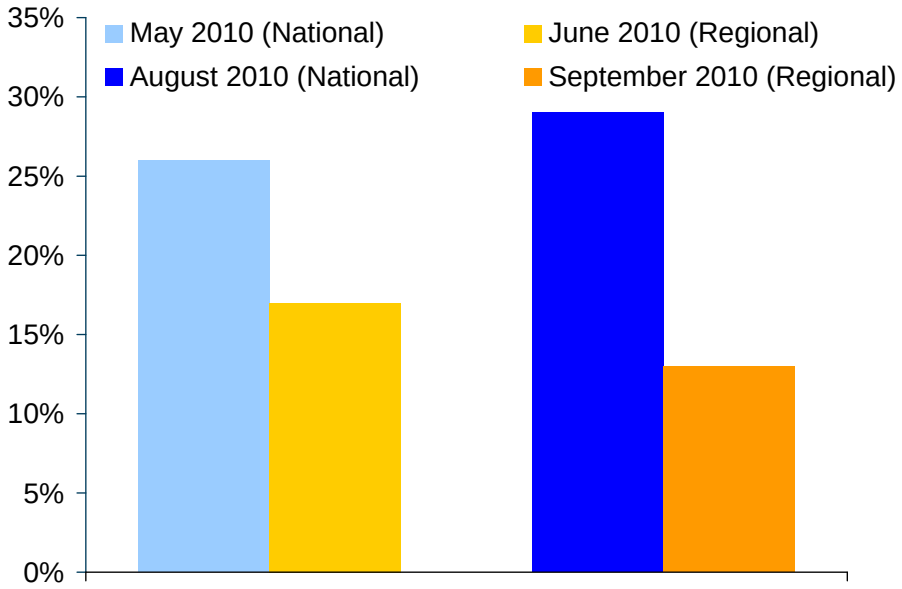

Source : MDRG/Louisiana Office of Tourism

Based on the available data, we estimate that total visitation to Louisiana declined 1% in the 2nd quarter. Business travel increased 17.6% over 2009 Q2 while leisure travel decreased 7.6%.

To arrive at the spending level of the initial impact we adjusted per visitor spending (by purpose of trip) based on the baseline forecast using data available for 2010 Q2. On a per trip basis, spending per visit increased modestly in the 2nd quarter from the prior year. This was driven both by increases in room rates and general price inflation overall.

Multiplying per visitor spending by the number of visitors provides us with visitor spending by purpose of trip. Our results show business travelers spent $68 million in 2010 Q2, representing an increase of 17.2% relative to the baseline forecast. Leisure travel spending tallied $1.4 billion, 9.2% below the baseline forecast. In total, visitor spending was $2.1 billion in 2010 Q2. Lost visitor spending is calculated at $42 million, 2.0% below the baseline forecast in the 2nd quarter.

Continuing effects from perceptions

The effects on Louisiana visitation related spending are expected to persist for some time. This is supported by research conducted by Tourism Economics on behalf of the US Travel Association which analyzed the impact of previous oil spills on tourism spending for affected destinations. The average range of impact duration for the five prior spills analyzed was between 12 and 28 months, with the Ixtoc spill impacts lasting 36 months.

Duration of Oil Spill Tourism Impacts

Months after initial disruption for visitor spending to return to baseline

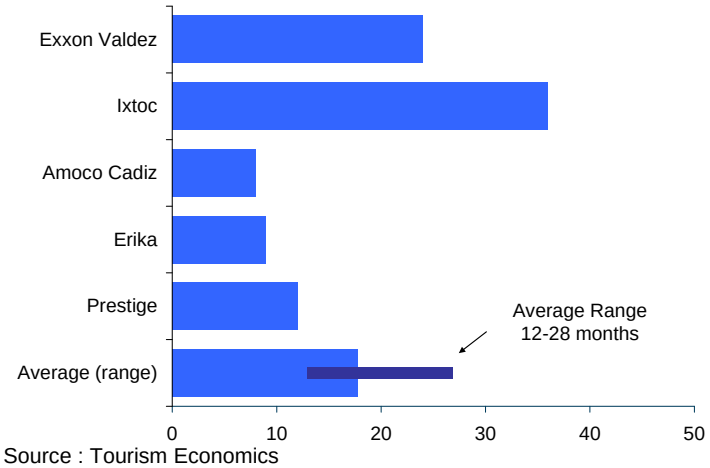

Source : Tourism Economics

Further evidence of lingering effects is suggested in survey results of leisure travelers, both national and regional, conducted for the Louisiana Office of Tourism by MDRG. These surveys were conducted in waves following the onset of the crisis. Not only do these surveys suggest that visitors had already cancelled or postponed planned trips to Louisiana in the following 12 months, but the May survey shows that perceptions regarding the recovery of Louisiana's tourism product would be long lived. Nearly 80% of national respondents believed the oil spill would affect Louisiana for 2 or more years. The percentage jumps to 88% from the regional survey which includes the majority of Louisiana's top source markets. The national survey conducted in August shows expectations declining with the distribution more closely related to the earlier regional survey.

Perception of Effect on Louisiana

% of respondents

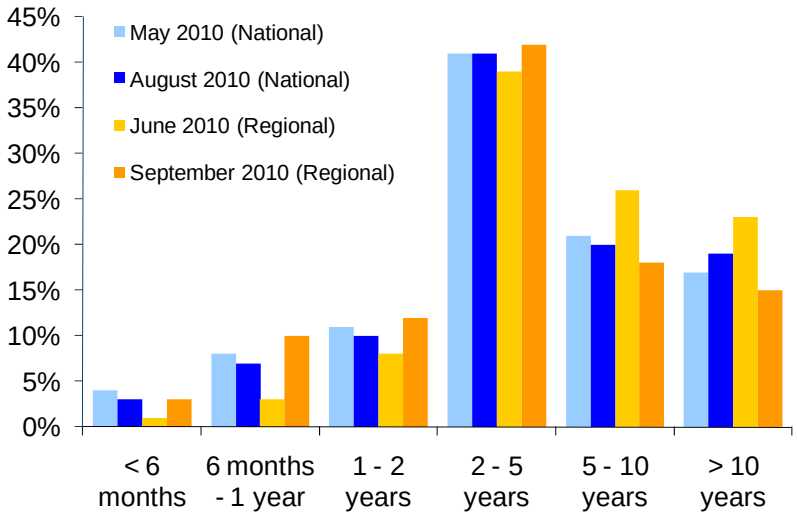

Source : MDRG/Louisiana Office of Tourism

Our model uses this distribution of perceptions as a starting point for estimating the recovery rate of leisure visitation over time. Looking at the chart, it is apparent that visitor perceptions initially recover slowly. Perceptions then rapidly improve after year two and then slow again as time progresses. If one were to plot this over time, one would expect to see a classic power- or S-curve. However, the effects on travel to Louisiana are not likely to be as long lived as suggested by the survey results. Thus, while our model exhibits the S-curve shape implied by the survey results, the duration of effects is shortened by applying the S-curve methodology only on the outstanding balance of "lost" visitors from the previous quarter as opposed to the initial impacts.

Thus, while our model exhibits the S-curve shape implied by the survey results, the duration of effects is shortened by applying the S-function only on the outstanding balance of "lost" visitors from the previous quarter as opposed to the initial impacts. To explain this more intuitively – once a visitor is "recovered" their perception of the destination is assumed to remain positive. Conversely, the "gained" business travel is expected to wane in a similar pattern. However, we expect that shape of the S-curve will be steeper. That is, the offsetting business travel related to the oil spill will decline at a faster rate than the recovery of leisure travelers. The model implies that visitor volumes should return to the baseline forecast in 2012 Q4.

Leisure Impact

% relative to baseline forecast

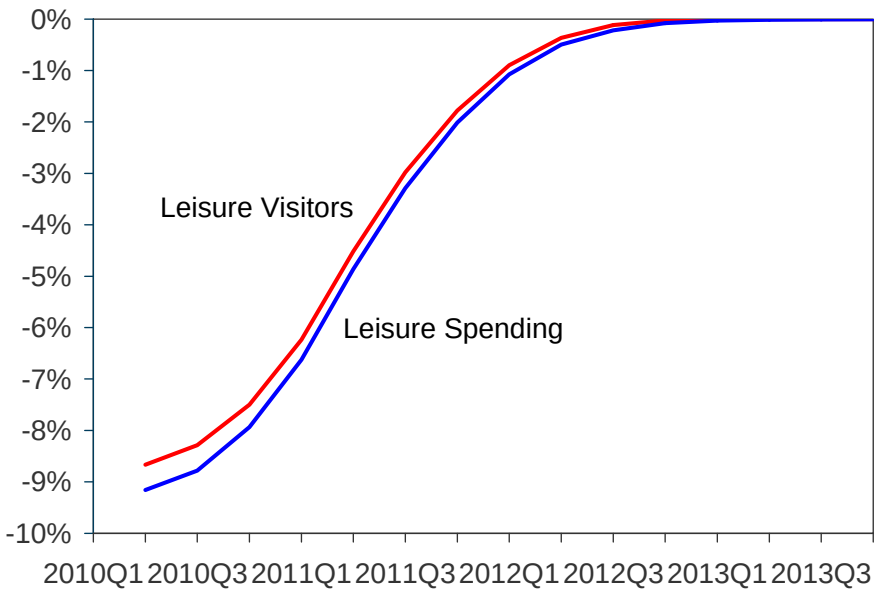

Source : Tourism Economics

Effects on visitor spending

Along with the decrease in visitor volume resulting from the disaster, per visitor spending was also assessed. In the face of decreased demand, purveyors of travel services are likely to lower prices to attract visitors. Thus, visitors can consume the same amount of services for an otherwise lower amount. This downward pressure on prices in the near term will delay

the return of spending relative to visitor volume. In addition, MDRG surveys indicate that visitors from nearby markets are less hindered than those from further away—who tend to stay longer and spend more per visit. Our model indicates that visitor spending will return the baseline by 2013 Q2, although the losses in spending in 2013 Q1 are expected to be only marginal. This would put the duration of effects on visitor spending at approximately 36 months.

Tracking the effects

The projection of impacts presented in this report remains open to both positive and negative risks. Visitor demand will vary based upon perceptions which will be affected by the revelation of new information over time and through the positive marketing of Louisiana. Perceptions are set to continue to improve though the possibility of additional shocks (e.g. oil washing ashore or evidence of tainted seafood) could send perceptions sliding. The results will also be refined and revised with the collection of historic data over time. Future updates to this report will incorporate any new data available to accurately assess the impacts on tourism spending.

Methodological notes

Seasonality is an important factor in determining the effects of a shock on tourism activity. To address seasonality, we use a quarterly model as the basis of our analysis. The baseline forecast, however, is an annual model which needed to be converted to a quarterly basis. Historical visitor volumes were seasonalized based on a weighted average of visitation by quarter from TNS data for Louisiana and STR data on room nights sold. A two year moving average was then used to seasonalize the forecast periods. Visitor spending was seasonalized using the US Travel Association's Travel Price Index.

Additionally, the baseline forecast was only available on an aggregated basis, i.e. total visits and total visitor spending. Thus, TNS data (from which the baseline forecast was partially derived) was used to disaggregate business and leisure visitation and spending.

AGU PUBLICATIONS

Geophysical Research Letters

RESEARCH LETTER
10.1002/2016GL071685

Key Points:
- The 3 September 2016, M_w 5.8 Pawnee earthquake is the largest event recorded in Oklahoma, rupturing along a previously unmapped basement fault
- In 2016, the rate of *M*3 and greater earthquakes in Oklahoma has decreased, but the cumulative moment has increased
- Observations from this and other Oklahoma earthquakes point to the difficulty in mitigation after years of fluid injection

Supporting Information:
- Supporting Information S1
- Table S3

Correspondence to:
W. L. Yeck,
wyeck@usgs.gov

Citation:
Yeck, W. L., G. P. Hayes, D. E. McNamara, J. L. Rubinstein, W. D. Barnhart, P. S. Earle, and H. M. Benz (2017), Oklahoma experiences largest earthquake during ongoing regional wastewater injection hazard mitigation efforts, *Geophys. Res. Lett.*, *44*, 711–717, doi:10.1002/2016GL071685.

Received 21 OCT 2016
Accepted 11 DEC 2016
Accepted article online 14 DEC 2016
Published online 21 JAN 2017

Oklahoma experiences largest earthquake during ongoing regional wastewater injection hazard mitigation efforts

W. L. Yeck[1], G. P. Hayes[1], D. E. McNamara[1], J. L. Rubinstein[2], W. D. Barnhart[3], P. S. Earle[1], and H. M. Benz[1]

[1]U.S. Geological Survey, National Earthquake Information Center, Denver, Colorado, USA, [2]U.S. Geological Survey, Earthquake Science Center, Menlo Park, California, USA, [3]Department of Earth and Environmental Sciences, University of Iowa, Iowa City, Iowa, USA

Abstract The 3 September 2016, M_w 5.8 Pawnee earthquake was the largest recorded earthquake in the state of Oklahoma. Seismic and geodetic observations of the Pawnee sequence, including precise hypocenter locations and moment tensor modeling, shows that the Pawnee earthquake occurred on a previously unknown left-lateral strike-slip basement fault that intersects the mapped right-lateral Labette fault zone. The Pawnee earthquake is part of an unprecedented increase in the earthquake rate in Oklahoma that is largely considered the result of the deep injection of waste fluids from oil and gas production. If this is, indeed, the case for the *M*5.8 Pawnee earthquake, then this would be the largest event to have been induced by fluid injection. Since 2015, Oklahoma has undergone wide-scale mitigation efforts primarily aimed at reducing injection volumes. Thus far in 2016, the rate of *M*3 and greater earthquakes has decreased as compared to 2015, while the cumulative moment—or energy released from earthquakes—has increased. This highlights the difficulty in earthquake hazard mitigation efforts given the poorly understood long-term diffusive effects of wastewater injection and their connection to seismicity.

1. Introduction

On 3 September 2016, the largest recorded earthquake in Oklahoma history (M_w 5.8) occurred approximately 15 km to the northwest of the town of Pawnee. The earthquake was felt across the Central United States up to distances over 1500 km, with multiple felt reports ranging from Denver, Colorado, to Chicago, Illinois. There are reports of one injury due to the earthquake and strong to severe damage (Modified Mercalli Intensity (MMI) VI–VIII) in the epicentral region. In addition to six buildings in Osage County reported as uninhabitable immediately after the earthquake [*Bustillo and Strum*, 2016], there were also reports of collapsed chimneys, damage to unreinforced brick masonry buildings, and damage to brick facades [*Clayton et al.*, 2016]. Postevent geological surveys observed sandblows and ground failure (slumping) in the epicentral region and minor evidence of ground cracking on a property ~3 km NE of main shock [*Clayton et al.*, 2016], and nearby stream discharge temporally increased near the event as a result of local changes to shallow hydrogeological properties [*Manga et al.*, 2016].

Before 2011, moderate (*M*5–6) earthquakes in Oklahoma were rare, with documented events occurring in 1882 and 1952 (Figure 1a) [*Hough and Page*, 2015]. Since November 2011, four *M*5+ earthquakes have occurred, including the 2011 M_w 5.7 Prague [*Keranen et al.*, 2013], 2016 M_w 5.1 Fairview [*Yeck et al.*, 2016], M_w 5.8 Pawnee, and M_w 5.0 Cushing earthquakes (Figure 1a). Since 2008, the rate of magnitude 3.5 and greater earthquakes in the Central United States has dramatically increased [*Ellsworth et al.*, 2015]. This change has been attributed to anthropogenic sources, predominantly from the subsurface injection of large volumes of wastewater related to oil and gas production [*Weingarten et al.*, 2015]. Wastewater injection likely caused both the Prague and Fairview, Oklahoma, earthquakes [*Keranen et al.*, 2013; *Yeck et al.*, 2016], and the overall seismicity rate increase throughout the Central United States [*Ellsworth*, 2013; *Walsh and Zoback*, 2015; *Weingarten et al.*, 2015]. As the Pawnee earthquake lies within a region of seismicity largely considered anthropogenic [*Langenbruch and Zoback*, 2016], and as other recent moderate earthquakes in Oklahoma have been linked to wastewater injection [*Keranen et al.*, 2013; *McNamara et al.*, 2015b; *Yeck et al.*, 2016], it is probable, but not certain, that the Pawnee sequence was induced. The anthropogenic nature of this event will not be clear until wastewater injection data from the region can be evaluated.

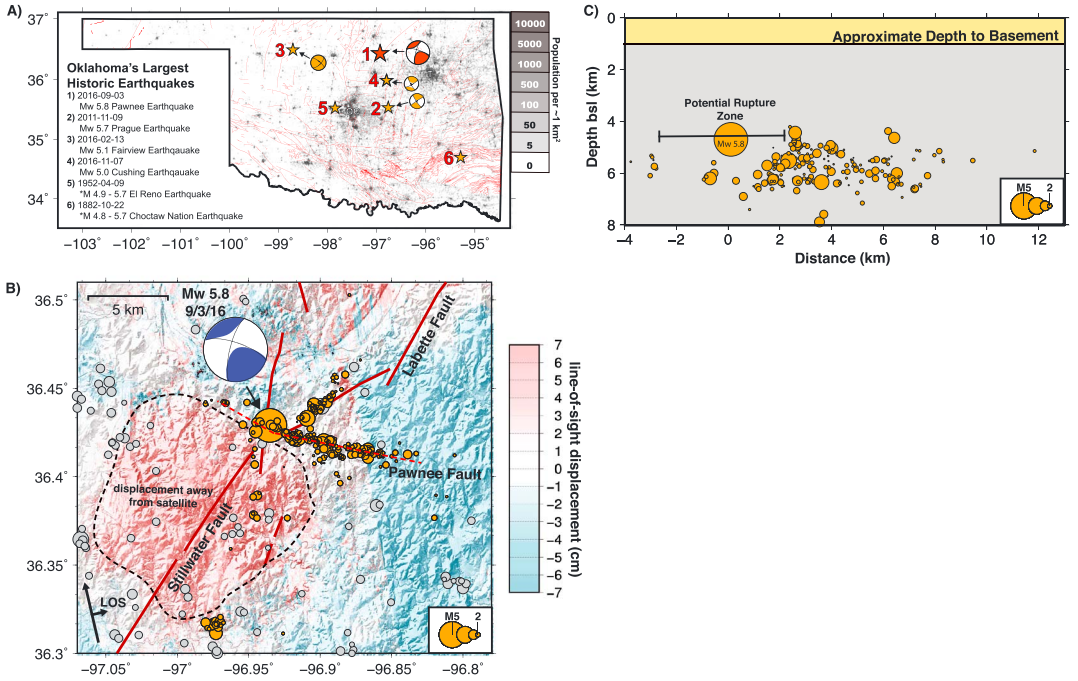

Figure 1. This figure shows an overview of moderate earthquakes in Oklahoma and details of the recent Pawnee earthquake sequence. (a) Map of largest historic earthquakes in Oklahoma (stars). Epicenter locations for the 1882 and 1952 events are from *Hough and Page* [2015]. The Pawnee, Prague, Fairview, and Cushing event locations are from National Earthquake Information Center. Mapped faults shown as red lines [*Holland*, 2015]. The background population density is shown from LandScan population database [*Bhaduri et al*., 2002]. (b) Map view of multiple-event relocation hypocenters surrounding Pawnee M_w 5.8 earthquake. The orange circles denote the aftershocks and the main shock. The gray circles denote the foreshocks. Previously mapped faults are shown as dark red lines [*Holland*, 2015]. The Pawnee fault, inferred from seismicity, is shown as red dashed lines. Region of uplift because of the Pawnee main shock, based on InSAR observations, is circled with black dashed line. (c) A cross section of seismicity within $\pm$2 km of the strike of the Pawnee fault (100°). The *x* axis shows the distance along strike centered on main shock, with positive values toward the east. Approximate depth to basement is shown as solid line from nearby well data [*Campbell and Weber*, 2006]. Details on earthquake relocation procedures are discussed in the supporting information.

2. Source Characteristics of the Pawnee Sequence

In an effort to better understand the seismotectonics and spatiotemporal variations in seismicity related to the Pawnee earthquake, the U.S. Geological Survey (USGS) deployed eight seismic stations near the main shock. We used these instruments to determine precise locations of the seismic sequence [e.g., *Jordan and Sverdrup*, 1981; *Hayes et al*., 2013; *McNamara et al*., 2015a, 2015b] (see supporting information). Aftershocks primarily occur along an ~7.5 km long, previously unmapped WNW-ESE trending fault, which we refer to as the Pawnee fault (Figure 1b). This fault crosses the northeast-southwest trending Labette fault zone [*Denison*, 1984] that is preferentially aligned for failure in the present-day crustal stress field [*Darold and Holland*, 2015]. Aftershocks also occur on the Labette fault north of the Pawnee fault. The Pawnee main shock hypocenter is located in the Precambrian basement at a depth of 4.7 $\pm$ 1.0 km. The majority of aftershocks in the Pawnee sequence are located at depths ranging from 5 to 7 km, suggesting that rupture primarily occurred in Precambrian basement (Figure 1c). Moment tensors derived by inverting the W phase [*Kanamori and Rivera*, 2008] (see supporting information) and regional surface waves [*Herrmann et al*., 2011] indicate strike-slip focal mechanisms with near-vertical nodal planes oriented on average 194°–197° and 289°–287°, consistent with the fault plane imaged by the aftershock locations (Figure 1b). Satellite-based interferometric synthetic aperture radar observations show a region of line-of-sight displacement adjacent to the Pawnee main shock (Figure 1b) consistent with a shallow left-lateral strike-slip earthquake (see supporting information). This region of surface deformation is near a zone of aftershocks surrounding the Pawnee main shock (Figure 1c). Aftershocks often are located near the periphery of major slip patches

[*Beroza and Zoback*, 1993]; therefore, the region of maximum slip may be bounded by the high-density zone of aftershocks east of the main shock (Figure 1c).

Coulomb failure stress change (ΔCFS) modeling indicates that a portion of the Labette fault zone which passes through Stillwater, Oklahoma, referred to herein as the Stillwater fault, may have been driven toward failure as a result of recent seismicity (see supporting information). We model positive ΔCFS of 0.025 MPa on the SW extension of the fault (Figure S1 in the supporting information). A positive stress increase of 0.01 MPa is sufficient to promote rupture on a critically stressed fault [*Stein*, 1999]. The Stillwater fault south of the Pawnee rupture location is a major fault system with an orientation favorable to slip [*Darold and Holland*, 2015], yet few aftershocks have occurred on the Stillwater fault, suggesting the structure may not be critically stressed. Still, the fact that this fault may have been driven closer toward failure by the Pawnee rupture emphasizes the compound nature of earthquake hazard in Oklahoma—the broad scale increased hazard related to wastewater injection activity, and the more localized hazard increase related to stress changes near induced earthquakes.

3. Observations from Four Moderate Earthquakes

Examining the four recent moderate Oklahoma earthquakes, we find a number of similarities. All four events occurred on near-vertical strike-slip faults in the shallow Precambrian basement. Similarly, each of the faults on which these earthquakes occurred on would be considered near optimally oriented for slip in the contemporaneous state of stress in Oklahoma [*Darold and Holland*, 2015; *Walsh and Zoback*, 2016].

However, the behaviors of the four sequences are different (Figure 2). The Prague, Fairview, and Cushing main shocks were preceded by relatively large foreshocks. The M_w 5.1 Fairview earthquake was preceded by six *M*4.0 or greater events in the 3 months before the main shock. Similarly, five M_w 4.0 and greater earthquakes preceded the Cushing M_w 5.0 main shock, although over 1 year passed between the last M_w 4+ earthquake and the Cushing M_w 5.0. The M_w 5.7 Prague event was preceded by a single M_w 4.8 foreshock the previous day, and the Pawnee earthquake occurred with nearly no foreshock activity, with only a single *M*3, or larger, earthquake in the preceding 60 days. The Pawnee main shock has produced fewer and smaller aftershocks, including 11 *M*3 and greater events in the 15 days following the main shock, the largest being a *M*3.9 (Figure 2). In contrast, in the 15 days following the Prague and Fairview earthquakes, there were 35 and 25 *M*3 and greater aftershocks and 2 and 1 *M*4 and greater aftershocks, respectively.

If the Pawnee earthquake turns out to have been induced by wastewater injection, then we have another interesting case history to add to those already in hand that can be used to evaluate the effectiveness of proposed hazard mitigation strategies. One suggested strategy is to limit injection near faults that are preferentially oriented to fail in the regional stress field [*Zoback*, 2012]. To this end, researchers have used a catalog of faults in Oklahoma in an effort to evaluate the locations of optimally oriented structures [*Holland*, 2013; *Darold and Holland*, 2015; *Walsh and Zoback*, 2016]. The M_w 5.7 Prague earthquake ruptured unmapped extensions of a mapped optimally oriented splay of the Wilzetta fault [*Keranen et al*., 2013; *McNamara et al*., 2015a] (Figure 2). Similarly, the M_w 5.1 Fairview earthquake ruptured on an unmapped extension of a previously documented optimally oriented fault [*Yeck et al*., 2016] (Figure 2). The M_w 5.8 Pawnee earthquake occurred on unknown splay of the Labette fault (Figure 2). The Cushing sequence has occurred primarily on two unmapped fault structures. The occurrence of relatively large earthquakes on unmapped structures demonstrates the difficulty of this approach in forecasting damaging earthquakes due to our incomplete knowledge of subsurface structures. Further complicating earthquake hazard mitigation is the fact that large-scale, high-volume wastewater injection in Oklahoma can result in distant ($>$10 km) pore pressure changes that induce earthquakes [e.g., *Keranen et al*., 2014; *Yeck et al*., 2016]. At best, the strategy of avoiding optimally oriented faults can reduce the probability of inducing an earthquake on known faults.

Another method used to reduce induced earthquake hazard uses a "traffic-light" system based on earthquake activity. These are commonly employed by regulatory agencies in an effort to reduce the occurrence of large earthquakes [*McGarr et al*., 2015] by reducing ("yellow-light") or stopping ("red-light") injection at wells near earthquakes of a specified size. The goal of this strategy is to reduce pore pressure changes where earthquakes are occurring. This type of strategy was employed in Cushing, Oklahoma, following a series of M_w 4 and greater earthquakes. In late 2015, injection wells within 3 km of the seismicity were directed to stop

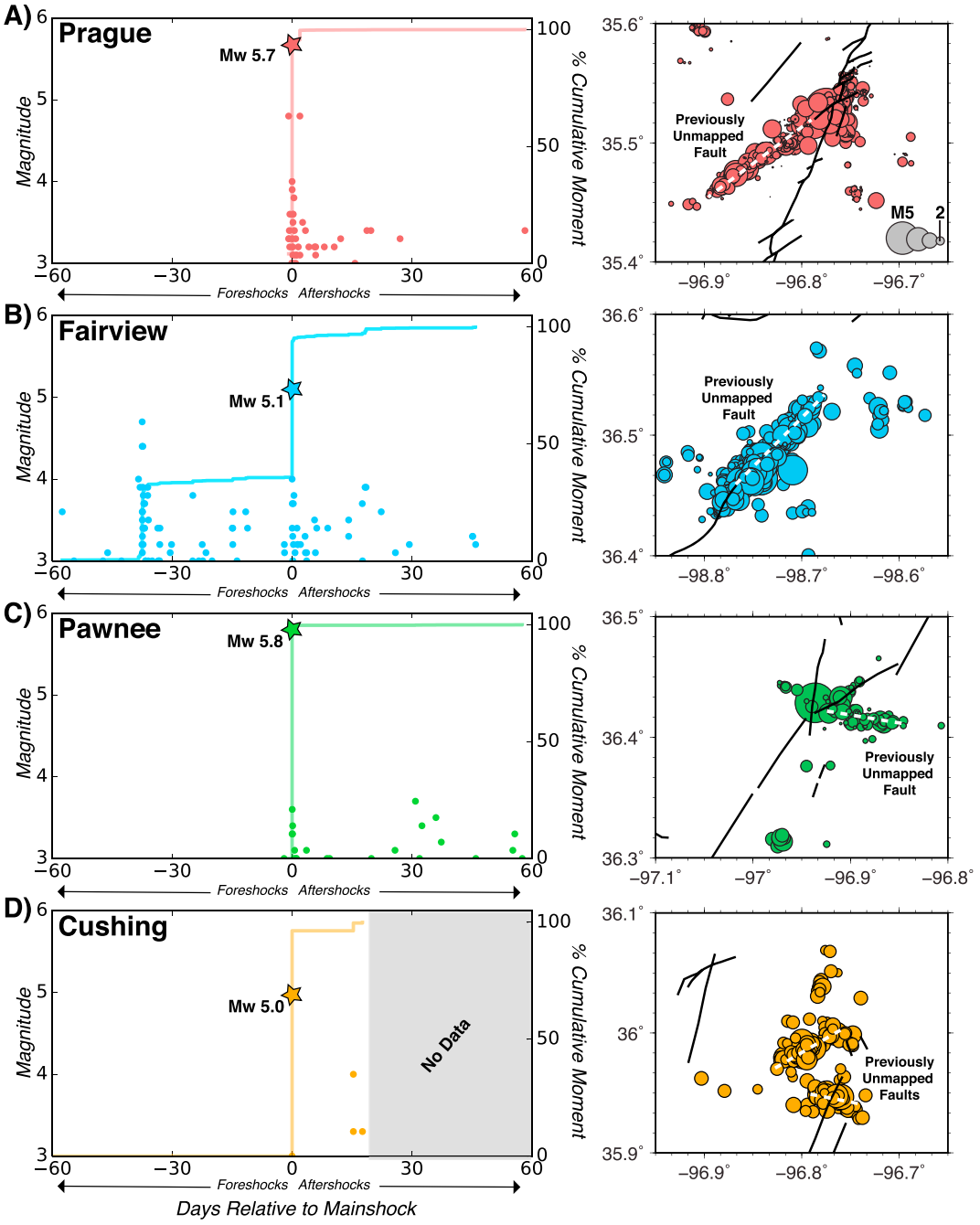

Figure 2. Plots show the distinct spatial and temporal characteristics of the four recent moderate earthquakes in Oklahoma. (left) A comparison of the foreshock and aftershock (≥*M*3) sequences relative to main shock date for the (a) Prague, (b) Fairview, (c) Pawnee, and (d) Cushing earthquakes, defined as events within 10 km of the main shock. The percentage of total cumulative moment for events shown as solid line. Individual events shown as dots and the main shocks are shown as stars. (right) The relocations of each sequence from previous studies [*McNamara et al.*, 2015a; *Yeck et al.*, 2016] and this study. Single-event solutions from NEIC shown for the Cushing sequence (https://earthquake.usgs.gov/earthquakes/search/, last accessed 28 November 2016). The white dashed lines show the inferred faults that were not mapped prior to seismicity. Mapped faults are shown as black lines [*Holland*, 2015].

injecting, and wells within 3–6 km were directed to reduce injection volumes [*Oklahoma Corporation Commission*, 2015]. Despite these efforts, a magnitude M_w 5.0 earthquake occurred on 7 November 2015, within the 3 km region of shut-in wells. The region of shut-in wells was extended following the M_w 5.0 event [*Oklahoma Corporation Commission*, 2016a].

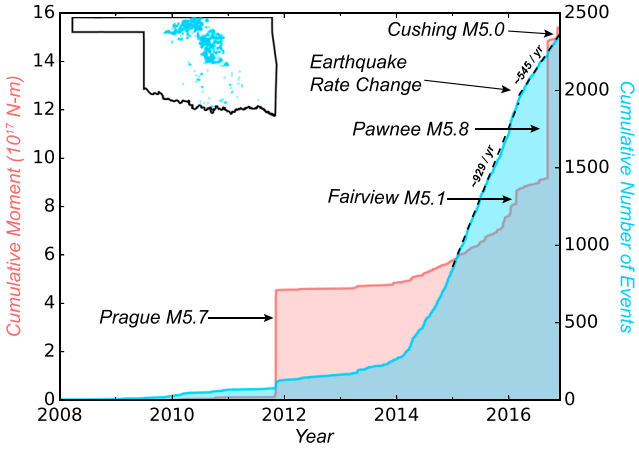

Figure 3. Cumulative moment (red) and cumulative number of events (blue) for all *M*3 and greater earthquakes in Oklahoma since 2000. Moment of major earthquakes is noted, as well as the recent rate change in *M*3 and greater events. Earthquake catalog from USGS COMCAT catalog (https://earthquake.usgs.gov/earthquakes/search/, last accessed 28 November 2016), with reported magnitudes converted to moment [*Kanamori*, 1977]. A map of the earthquakes is shown in top left corner. Average rates (black dashed lines) are calculated from time ranges 1 January 2015 to 6 March 2016 and 7 March to 28 November 2016.

It is unlikely that this kind of traffic-light strategy would have worked for the Fairview sequence, which also had protracted vigorous foreshock activity, as the Fairview earthquakes were predominantly induced by disposal wells greater than 10 km away from seismicity, and therefore, instantaneous changes at these wells would have a delayed effect on pore pressures in the far field [*Yeck et al.*, 2016]. The M_w 5.7 Prague earthquake only had foreshocks in the 1 day preceding it (Figure 2). Although the Prague foreshock was large (M_w 4.8), it is unlikely that changes to operations could be made rapidly enough to affect earthquake triggering the following day. If induced, the Pawnee earthquake would also not be a viable candidate for this approach to mitigating hazard, as in the previous 60 days only one *M*3+ (a *M*3.2) earthquake occurred. Given that 181 *M*3.2 or larger earthquakes have occurred throughout central Oklahoma in 2016 (through 1 September) unrelated to sequences hosting damaging events (Fairview), using such a small earthquake as a method to forecast future events would not be effective. Such a low threshold would produce a near-constant state of alert.

Regional injection reduction or cessation is another possible mitigation strategy. Questions still remain about how effective this strategy is over a short time frame as fluid pressures may remain high for years and propagate over great distances, especially in the case of long-duration injection operations [*McGarr et al.*, 2015]. In fact, it is well documented that seismicity can continue long after the cessation of injection. For example, the largest of the "Denver earthquakes" occurred more than 1 year after injection was terminated [*Healy et al.*, 1968]. More recently, seismicity rates have been observed to increase while injection rates decreased near Timpson, Texas, due to the slow propagation of the fluid-pressure pulse [*Frohlich et al.*, 2014; *Shirzaei et al.*, 2016].

4. Conclusion

The Oklahoma Corporation Commission (OCC) has either advised or mandated the reduction or cessation of disposal down many wells in Oklahoma surrounding regions of elevated seismicity, and therefore, we are in the midst of a large-scale experiment in how injection reduction affects seismicity on a local and regional scale. The OCC implemented a large-scale injection reduction plan on 7 March 2016, with a goal of reducing the annual volume of injection in an ~26,000 km^2 region to 40% of the 2014 total [*Oklahoma Corporation Commission*, 2016b]. This region included the locations of the subsequent Pawnee and Cushing earthquakes. Seismicity rates throughout Oklahoma (measured in terms of total number of earthquakes above *M*3 per unit time) have declined in 2016 relative to 2015 [*Langenbruch and Zoback*, 2016], but the seismic moment rate has increased (Figure 3), largely due to the Pawnee, Fairview, and Cushing earthquakes. Since the Pawnee earthquake, the OCC, and Environmental Protection Agency (which has regulatory authority in nearby Osage County) issued mandatory directives that 32 wastewater disposal wells near the Pawnee main shock epicenter cease operations and 35 wells reduce injection volumes [*Oklahoma Corporation Commission*, 2016c].

It is well recognized that reductions in wastewater injection will not have an instantaneous effect on seismicity rates [*Langenbruch and Zoback*, 2016; *Oklahoma Corporation Commission*, 2016b]. While the effectiveness

of the ongoing mitigation strategies in Oklahoma on the occurrence of moderate earthquakes remains to be seen, it is possible to estimate the short-term hazard presented by induced earthquakes. In this effort, the USGS produced an induced earthquake seismic hazard forecast for 2016 [*Petersen et al.*, 2016]. Maximum observed shaking intensity (MMI VII–VIII) and damage reports in the epicentral region of the 2016 M_w 5.8 Pawnee, M_w 5.1 Fairview, and M_w 5.0 Cushing earthquakes are consistent with the forecast for central Oklahoma. This suggests that such short-term hazard models may act as a reasonable guide for where mitigation efforts might be focused.

Acknowledgments

The authors thank Art McGarr, George Choy, Jake Walter, and Manoo Shirzaei for their thoughtful reviews. The authors thank the USGS field teams from the Albuquerque Seismological Laboratory and Pasadena office for the rapid deployment of aftershock seismic monitoring systems (D. Wilson, S. Ploetz, D. Worley, C. Defario, and J. De Cristofaro). Authors also thank staff at the Oklahoma Geological Survey, Oklahoma State University, Cornell University, and Lamont-Doherty Earth Observatory for the coordination and cooperation on instrument deployments. All of the USGS waveform data and associated station metadata used in this study are archived and available for download from the IRIS Data Management Center. Earthquake source parameters used, including phase arrival time data, are available in the USGS Comprehensive Catalog of Earthquakes (http://earthquake.usgs.gov/earthquakes/map/). The relocated earthquake catalog and velocity model used in this study can be found in the supporting information and is also archived in the USGS ScienceBase (https://www.sciencebase.gov/catalog/). Any use of trade, firm, or product names is for descriptive purposes only and does not imply endorsement by the U.S. Government. Copernicus Sentinel data were retrieved from the ESA Scientific Data Hub and Alaska Satellite Facility DAAC in September 2016.

References

Beroza, G. C., and M. D. Zoback (1993), Mechanism diversity of the Loma–Prieta aftershocks and the mechanics of mainshock-aftershock interaction, *Science*, *259*, 210–213, doi:10.1126/science.259.5092.210.

Bhaduri, B. L., E. A. Bright, P. Coleman, and J. Dobson (2002), LandScan: Locating people is what matters, *Geoinformatics*, *5*(2), 34–37.

Bustillo, M., and B. Strum (2016), Oklahoma earthquake felt in several U.S. states, as oil wells draw scrutiny, *Wall Str. J.*

Campbell, J. A., and J. L. Weber (2006), *Wells Drilled to Basement in Oklahoma*, Oklahoma Geological Survey, Norman.

Clayton, P., G. Zalachoris, E. Rathje, T. Bheemasetti, S. Caballero, X. Yu, and S. Bennett (2016), *The Geotechnical Aspects of the September 3, 2016 M*5.8 Pawnee, Oklahoma Earthquake, GEER Association, doi:10.18118/G69885.

Darold, A. P., and A. A. Holland (2015), Preliminary Oklahoma optimal fault orientations (OF4-2015).

Denison, R. E. (1984), Basement rocks in northern Arkansas, *Contrib. Geol. Arkansas*, *2*, 33–49.

Ellsworth, W. L. (2013), Injection-induced earthquakes, *Science*, *341*(6142, 1225942), doi:10.1126/science.1225942.

Ellsworth, W. L., A. L. Llenos, A. F. Mcgarr, A. J. Michael, J. L. Rubinstein, C. S. Mueller, M. D. Petersen, and E. Calais (2015), Increasing seismicity in the U. S. midcontinent: Implications for earthquake hazard, *Leading Edge*, *34*(6), 618–620, doi:10.1190/tle34060618.1.

Frohlich, C., W. Ellsworth, W. A. Brown, M. Brunt, J. Luetgert, T. MacDonald, and S. Walter (2014), The 17 May 2012 *M* 4.8 earthquake near Timpson, East Texas: An event possibly triggered by fluid injection, *J. Geophys. Res. Solid Earth*, *119*, 581–593, doi:10.1002/2013JB010755.

Hayes, G. P., E. Bergman, K. L. Johnson, H. M. Benz, L. Brown, and A. S. Meltzer (2013), Seismotectonic framework of the 2010 February 27 M_w 8.8 Maule, Chile earthquake sequence, *Geophys. J. Int.*, *195*(2), 1034–1051, doi:10.1093/gji/ggt238.

Healy, J. H., W. W. Rubey, D. T. Griggs, and C. B. Raleigh (1968), The Denver earthquakes, *Science*, *161*(3848), 1301–1310, doi:10.1126/science.161.3848.1301.

Herrmann, R. B., H. Benz, and C. J. Ammon (2011), Monitoring the earthquake source process in North America, *Bull. Seismol. Soc. Am.*, *101*(6), 2609–2625, doi:10.1785/0120110095.

Holland, A. A. (2013), Optimal fault orientations within Oklahoma, *Seismol. Res. Lett.*, *84*(5), 876–890, doi:10.1785/0220120153.

Holland, A. A. (2015), Preliminary fault map of Oklahoma (OF3-2015).

Hough, S. E., and M. Page (2015), A century of induced earthquakes in Oklahoma?, *Bull. Seismol. Soc. Am.*, *105*(6), 2863–2870, doi:10.1785/0120150109.

Jordan, T. H., and K. A. Sverdrup (1981), Teleseismic location techniques and their application to earthquake clusters in the south-central Pacific, *Bull. Seismol. Soc. Am.*, *71*(4), 1105–1130.

Kanamori, H. (1977), The energy release in great earthquakes, *J. Geophys. Res.*, *82*(20), 2981–2987, doi:10.1029/JB082i020p02981.

Kanamori, H., and L. Rivera (2008), Source inversion of W phase: Speeding up seismic tsunami warning, *Geophys. J. Int.*, *175*(1), 222–238, doi:10.1111/j.1365-246X.2008.03887.x.

Keranen, K. M., H. M. Savage, G. A. Abers, and E. S. Cochran (2013), Potentially induced earthquakes in Oklahoma, USA: Links between wastewater injection and the 2011 M_w 5.7 earthquake sequence, *Geology*, *41*(6), 699–702, doi:10.1130/G34045.1.

Keranen, K. M., M. Weingarten, G. A. Abers, B. A. Bekins, and S. Ge (2014), Induced earthquakes. Sharp increase in central Oklahoma seismicity since 2008 induced by massive wastewater injection, *Science*, *345*(6195), 448–51, doi:10.1126/science.1255802.

Langenbruch, C., and M. D. Zoback (2016), How will induced seismicity in Oklahoma respond to decreased saltwater injection rates?, *Sci. Adv.*, *2*(11), e1601542, doi:10.1126/sciadv.1601542.

Manga, M., C. Wang, and M. Shirzaei (2016), Increased stream discharge after the 3 September 2016 M_w 5.8 Pawnee, Oklahoma earthquake, *Geophys. Res. Lett.*, *43*, 11,588–11,594, doi:10.1002/2016GL071268.

McGarr, A., et al. (2015), Coping with earthquakes induced by fluid injection, *Science*, *347*(6224), 830–831, doi:10.1126/science.aaa0494.

McNamara, D. E., H. M. Benz, R. B. Herrmann, E. A. Bergman, P. Earle, A. Holland, R. Baldwin, and A. Gassner (2015a), Earthquake hypocenters and focal mechanisms in central Oklahoma reveal a complex system of reactivated subsurface strike-slip faulting, *Geophys. Res. Lett.*, *42*, 2742–2749, doi:10.1002/2014GL062730.

McNamara, D. E., et al. (2015b), Reactivated faulting near Cushing, Oklahoma: Increased potential for a triggered earthquake in an area of United States strategic infrastructure, *Geophys. Res. Lett.*, *42*, 8328–8332, doi:10.1002/2015GL064669.

Oklahoma Corporation Commission (2015), Media advisory—Cushing earthquakes. [Available at http://www.occeweb.com/News/10-19-15CUSHING 2.pdf.]

Oklahoma Corporation Commission (2016a), Advisory4—Cushing. [Available at https://www.occeweb.com/News/2016/11-08-16CUSHING PLAN.pdf.]

Oklahoma Corporation Commission (2016b), Media advisory—Regional earthquake response plan for central Oklahoma and expansion of the area of interest. [Available at https://www.occeweb.com/News/2016/03-07-16ADVISORY-AOI, VOLUME REDUCTION.pdf.]

Oklahoma Corporation Commission (2016c), Media advisory—Latest action regarding Pawnee area. [Available at http://www.occeweb.com/News/2016/09-12-16Pawnee Advisory.pdf (Accessed 1 January 2016).]

Petersen, M. D., C. S. Mueller, M. P. Moschetti, S. M. Hoover, A. L. Llenos, W. L. Ellsworth, A. J. Michael, J. L. Rubinstein, A. F. McGarr, and K. S. Rukstales (2016), Seismic-hazard forecast for 2016 including induced and natural earthquakes in the Central and eastern United States, *U.S. Geol. Surv. Open File Rep., 2016–1035*, 52 p., doi:10.3133/ofr20161035.

Shirzaei, M., W. L. Ellsworth, K. F. Tiampo, P. J. Gonzalez, and M. Manga (2016), Surface uplift and time-dependent seismic hazard due to fluid injection in eastern Texas, *Science*, *353*(6306), 1416–1419, doi:10.1126/science.aag0262.

Stein, R. S. (1999), The role of stress transfer in earthquake occurrence, *Nature*, *402*, 605–609.

Walsh, F. R., and M. D. Zoback (2015), Oklahoma's recent earthquakes and saltwater disposal, *Sci. Adv.*, 1–9, doi:10.1126/sciadv.1500195.

Walsh, F. R., and M. D. Zoback (2016), Probabilistic assessment of potential fault slip related to injection-induced earthquakes: Application to north central Oklahoma, USA, *Geology*, *44*(12), 1–4, doi:10.1130/G38275.1.

Weingarten, M., S. Ge, J. W. Godt, B. A. Bekins, and J. L. Rubinstein (2015), High-rate injection is associated with the increase in U.S. mid-continent seismicity, *Science*, *348*(6241), 1336–1340, doi:10.1126/science.aab1345.

Yeck, W. L., M. Weingarten, H. M. Benz, D. E. Mcnamara, E. Bergman, R. B. Herrmann, J. Rubinstein, and P. S. Earle (2016), Far-field pressurization likely caused one of the largest injection induced earthquakes by reactivating a large pre-existing basement fault structure, *Geophys. Res. Lett.*, *43*, 10,198–10,207, doi:10.1002/2016GL070861.

Zoback, M. D. (2012), Managing the seismic risk posed by wastewater disposal, *Earth Mag*, *2*, 38–43.

OXFORD
Abbey House, 121 St Aldates
Oxford, OX1 1HB, UK
Tel: +44 1865 268900

NEW YORK
817 Broadway, 10th Floor
New York, NY 10003, USA
Tel: +1 646 786 1863

LONDON
Broadwall House, 21 Broadwall
London, SE1 9PL, UK
Tel: +44 207 803 1400

SINGAPORE
No.1 North Bridge Road
High Street Centre #22-07
Singapore 179094
Tel: +65 6338 1235

email: mailbox@oxfordeconomics.com

www.oxfordeconomics.com

TOURISM ECONOMICS

Analysis of Casing Deformations in Thermal Wells

Jueren Xie and Yu Liu

C-FER Technologies, Edmonton, Alberta, Canada

Abstract: *Thermal technologies are widely used for the heavy oil recovery. The thermal processes usually consist of some variation of Cyclic Steam Stimulation (CSS), steam flood or Steam Assisted Gravity Drainage (SAGD). These thermal recovery applications have experienced numerous well casing failures around the world, often resulting in loss of wellbore integrity, lost production and added costs. The primary casing failure mechanisms include casing connection leakage and/or parting due to excessive casing strain and wellbore serviceability difficulties due to large casing deformation associated with casing buckling and shear.*

Due to high operation temperatures (e.g. 220 to 350°C), casing deformations often exceed the elastic limit of typical thermal well casing materials. Therefore, a strain-based design concept and advanced finite element analysis are often used to consider the allowable casing strain capacity beyond yield and the associated non-linear material and structural responses. This paper presents analysis models, developed using Abaqus, for analyzing casing deformations resulting from thermal loading, buckling and formation shear movement. It is demonstrated that the analysis results of casing deformations can constitute a more advanced and sound basis for thermal well casing designs which minimize the potential for thermal wellbore casing failures.

Keywords: *Casing, Connection, Thermal Well, Thermal Cycle Loading, Buckling, Formation Shear, Plasticity, Strain-based Design, Axisymmetric-Asymmetric Elements, Beam Elements, Slide-line Contact Elements, Pipe-in-Pipe Contact Elements*

1. Introduction

Thermal technologies are widely used for heavy oil recovery worldwide. The thermal recovery of viscous heavy oil and bitumen is often achieved by some variation of Cyclic Steam Stimulation (CSS), steam flood or Steam Assisted Gravity Drainage (SAGD). A thermal cycle in CSS consists of four basic phases: high pressure, high temperature steam injection; a soak period, where the well is shut-in to allow for the injected steam to penetrate the reservoir and decrease the oil viscosity; flow-back, where the elevated reservoir pressure is sufficient to produce the hot oil, condensed steam and gases to surface; and pumping to lift the produced fluids to surface as the reservoir cools. SAGD is a more stable, gentle process where steam is continuously injected into one horizontal well, and condensed steam and mobilized fluids are produced from a second well (Xie, 2000). This method usually requires lower injection pressures and temperatures and fewer pressure/temperature cycles than CSS. The CSS process has been applied to a variety of well configurations including vertical, directional and horizontal as shown in Figure 1. SAGD applications are typically limited to pairs of parallel horizontal wells with the dedicated injector situated just above the dedicated producing well (Figure 2).

Visit the SIMULIA Resource Center for more customer examples.

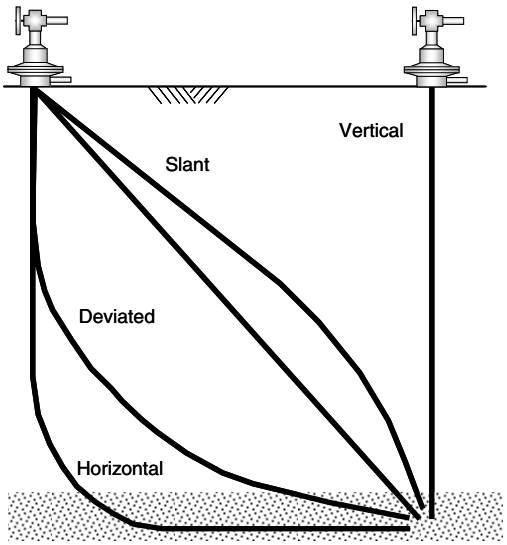

Figure 1. Straight and directional wells.

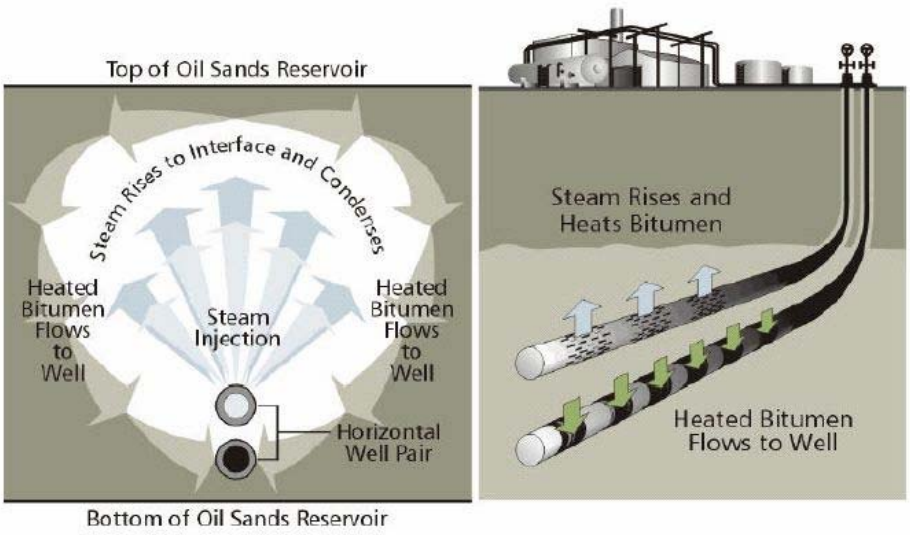

Figure 2. Casing strings used in producing well and steam injection well for the SAGD (Steam Assisted Gravity Drainage) process.

Thermal well production poses serious challenges to well casing designs. In addition to the installation loads, such as hanging/buoyancy forces and bending resulting from well curvature, a

casing must support the thermal strains resulting from large temperature variations and formation movements induced by thermal effects and well production. In many field operations, the temperature cycles impose cyclic compressive casing stress during heating and tensile stress during cooling. When "ultra-high temperature" is used (for example, peak temperatures over 300°C, depending on casing grade), the casing can potentially yield under tensile stress during cool-down, leading to possible failure modes of low cycle material fatigue, connection leakage and connection parting. In addition to the cyclic stress-temperature response, several field observations have suggested that casings can be subjected to curvature loads, such as casing buckling due to thermal compressive stress and shear deformation due to formation shear movement (Xie, 2000).

Thermal well casing designs often require advanced finite element analyses to consider the effects of temperature and stress on material properties and the plastic, non-linear response of the materials. The casing constitutive model must consider the elastic-plastic response of the material, temperature dependence and time dependence. This paper presents modeling and analysis considerations using the finite element program Abaqus to aid the thermal wellbore designer by simulating thermal well casing responses for various load conditions and casing design options. In addition, this paper presents finite element models for analyzing casing buckling and curvature response to formation shear movements.

2. Casing Failure Mechanisms and Design Considerations

Excessive casing deformations leading to failure of steam stimulation wells have been documented in literature (IOL Report, 1977; CNRL Report, 2000; Fu, 2006). The majority of these casing failures are noted to be the result of casing connection parting due to material failure in the stress concentration areas in casing connections. Some well failures occurred at the interface between the producing zone and the overlying shales and have been attributed to shear movement along what is assumed to be a very low friction boundary between the two formations (Xie, 2000). One theory to account for these failures is that the production-induced heat caused thermal expansion of the formations, resulting in a formation shear movement.

Figure 3 shows a multi-sensor caliper survey (Xie, 2000) of a CSS well which displays deformations consistent with multi-wave buckling and shear displacement (lateral displacements have been magnified for illustrative purposes). The shear displacement of the casing has a resulting wellbore curvature or "dogleg severity" exceeding 1000°/30 m. This high local curvature translates to a flexural strain on the outside diameter of the casing of over 5%, which is sufficient to fail a casing connection.

Traditional methods for casing structural design use the stress-based design concept which limits the casing stress to the elastic state. However, in many design cases for thermal well casings, the magnitudes of casing strains resulting from thermal loading, casing buckling and formation movement exceed the elastic strain limit, making the conventional stress-based design method inappropriate for these applications.

Today's well design practices acknowledge that limited plastic strain is acceptable for casings provided that the driving forces are displacement-controlled. The thermal strain and formation movements are controlled and bounded by the magnitude of the well temperature and the lithology and operating conditions of the application. The allowable casing strain is often defined by wellbore serviceability limits or failure criteria and the structural integrity of casing connections. It is important to note that the casing strain limit does not directly correlate with the requirement for connection sealability; that is, a connection may leak even if it is not loaded.

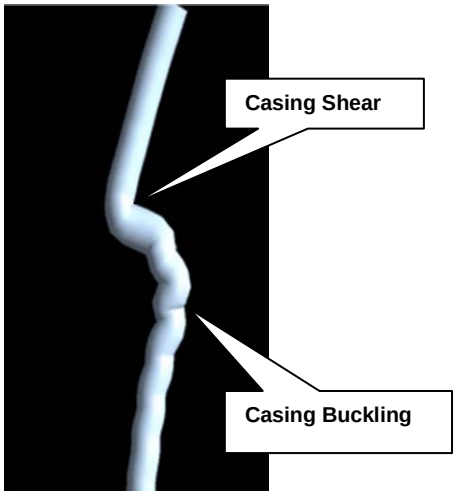

Figure 3. Multi-sensor caliper survey of casing buckling and shear in a cyclic steam stimulation well.

Based on the understanding of casing failure mechanisms, the casing design objectives proposed for thermal wells are as follows:

- Structural integrity to withstand the following:
  - **a.** thermal strain and internal/external pressures from the fluids and lithology;
  - **b.** casing buckling deformation caused by thermal compressive loading in cement void intervals; and
  - **c.** formation shear movement in the overburden and reservoir intervals.
- Connection sealability to withstand thermal loading, casing buckling and formation shear movements.

Note that the three structural integrity design objectives are examined in this paper while connection sealiability is not, in part because it is dependent on proprietary casing connection designs and there are several such designs available.

3. Analysis of Casing under Thermal Cycle Loading

3.1 Description of Loads

One of the key features in thermal wells is the large temperature change subjected to the well during normal operations. During steam injection periods, the temperature increases along the wellbore from as low as initial reservoir values of 10 to 25°C to peak temperatures of 220 to 275°C for SAGD wells, and 330 to 350°C for CSS wells. Assuming that the cement and formation provide sufficient axial constraint to axial movement, the temperature-induced thermal expansion of casing material will introduce significant axial compressive loading to the casing string. In the late part of a thermal cycle or during well servicing, when temperature decreases from the production peak value, the axial compressive force in casings may reverse to tensile force if the temperature drops sufficiently.

3.2 Analysis Models for Casing Material Response to Thermal Loading

Analysis of cyclic plastic/creep casing deformation in thermal wells requires a sophisticated finite element material model to account for the kinematic strain hardening deformation, or the Bauschinger effect, stress-relaxation and creep strain. Several researchers (Ellyin, 1995; Xia, 1997; Kaiser, 2005) have studied the mechanical properties of casing materials under cyclic loading conditions numerically and experimentally. It is generally acknowledged that the modified Mroz plasticity theory (Mroz, 1967) would be a better suited approach for modeling casing material response to plastic cyclic loading for thermal wellbore casing materials. However, the numerical attempts revealed a number of modeling issues that need to be resolved, especially when the problems involved cyclic plasticity and creep behavior of materials. These investigations indicated that, due to limitations of constitutive modeling, it is impractical to rely strictly on numerical analyses for casing cyclic plasticity deformation assessments.

A more simplistic and practical approach would be to assess casing design based on analyses of casing material response under monotonic or single cycle load conditions. Such analyses can be performed using established constitutive models available in many finite element programs, including Abaqus. Such simplified models should represent the stress-strain behavior in the casing materials in both elastic and plastic regions and across the entire spectrum of operating temperature of the analysis. It is therefore essential that the elastic-plastic constitutive model be defined as temperature and strain-rate dependent. Physical tests demonstrated that casing material yield strength usually decreases with temperature, and tensile strength may increase with temperature at the beginning of heating but decrease with further heating (Humphreys et al., 1991). Proper consideration of the strain-rate dependence of the material is necessary in order to simulate the stress relaxation phase of a thermal cycle.

3.3 Analysis Example

Consider a Western Canada SAGD well completion design that has a peak temperature of 275°C and an internal pressure of 2 MPa. The proposed design uses an L80 production casing, which is common for these applications. Finite element analysis is performed to determine the casing stress-strain response over the thermal cycle. This involves heating the casing from 10°C to

275°C and cooling back to 10°C. Figure 4 presents the relationship between the casing stress, plastic strain and temperature over the thermal cycle. The casing mechanical response to the thermal cycle consists of four loading stages:

1. During initial heating, the confined (cemented) casing material is compressed elastically until the elastic limit is reached in compression at approximately 196°C;
2. Further heating leads to plastic deformation (in this example, up to approximately 0.092%) due to the constrained thermal expansion;
3. As the casing is held constant at high temperature (275°C), stress relaxation occurs due to the development of creep strain; and
4. When the confined casing is cooled (from 275°C to 10°C), the axial load gradually changes from compression to tension.

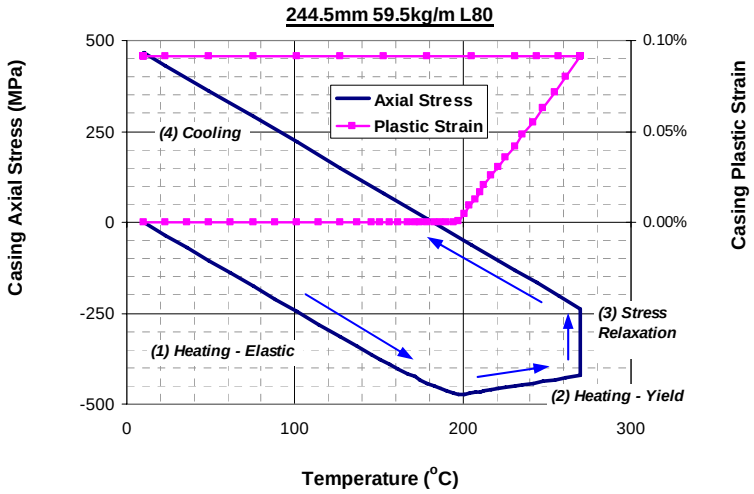

Figure 4. Stress and plastic strain over a thermal cycle for L80 casing material.

Figure 4 shows that the plastic strain starts to develop at 196°C and increases to approximately 0.092% at 275°C. In this case, there is no incremental plastic strain in the cooling stage or in any subsequent thermal cycles over this temperature range. It should be noted that in the case of "ultra-high temperature" production (i.e. up to 350°C), some casing materials (such as K55 and L80) may reach yield in tension at the end of a cycle (Xie, 2006). This will lead to incremental plastic deformation in further cycles, making low-cycle fatigue a critical failure mode of the casing, especially for CSS wells.

4. Analysis of Casing Buckling in Cement Voids

4.1 Description of Loads

The axial loads resulting from thermal expansion of the casing can cause casing buckling where lateral support for the casing is not provided (e.g. due to a void in the cement sheath). The buckling mode can vary from a single in-plane "bow" to a continuous series of "corkscrews" (helical buckle) depending on the magnitude of axial strain (Xie, 2006). Figure 5 illustrates the development of in-plane and helical buckling modes with increasing axial strain. The casing string can buckle at high temperature due to large compressive forces caused by thermal expansion. As the casing cools from the peak temperature, the casing buckling curvature will decrease as the casing goes into tension. However, some residual curvature resulting from the plastic buckling deformation will remain in the casing even at the end of a thermal cycle.

The assessment of casing resistance to buckling is important for two reasons. First, the casing may fail in connections due to excessive plastic strain associated with severe buckling. Second, well serviceability/accessibility may be impaired due to large casing curvature induced by buckling.

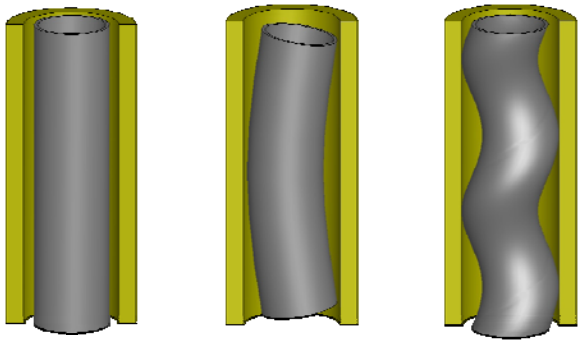

(a) Initial configuration | (b) In-plane buckling mode | (c) Helical buckling mode

Figure 5. Illustrative representation of casing buckling development in a cement void interval.

4.2 Analysis Models

Figure 6 shows a schematic representation of the finite element model developed for the casing buckling analyses. The casing was modeled using three-dimensional beam elements capable of simulating large deformations. It was assumed that a discrete annular gap exists between the casing outside diameter and the adjacent cement or formation to represent a void region (e.g. as might occur for a thermal well with a poorly-cemented interval). The outer radial boundary (e.g. formation interface) over the unsupported interval was conservatively assumed to be very stiff, thus providing rigid radial support for the casing if it deformed sufficiently to contact

the borehole wall. The interaction between the casing and the rigid borehole was modeled using pipe-in-pipe contact elements. Initial geometric imperfections in a helical mode should be assumed prior to the buckling analysis. Note that temperature variation and the resulting thermally-induced loads were the only loading conditions applied to this casing model in the buckling analysis.

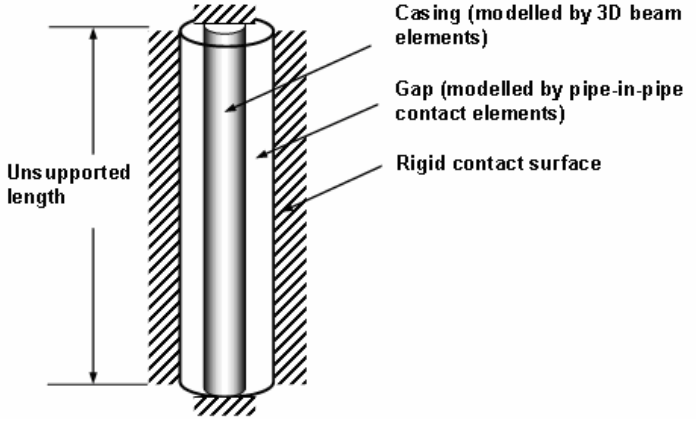

Figure 6. Schematic of finite element model for casing buckling analysis.

4.3 Analysis Example

The following analysis example is presented here to illustrate the application of this model for the consideration of potential casing buckling. This example considered the buckling of a 244.5 mm, 59.5 kg/m L80 casing under the thermal cycle loading noted above. Figure 7 shows the impact of temperature on the average axial stress and the resulting curvature and plastic strain experienced by the unsupported casing segment, with a cement void gap of 5 mm. Casing buckling initiates immediately after the casing yields during heating, shown in Figure 7 by a sharp increase in local curvature. With continued heating and thermal expansion, the initial in-plane buckling mode transforms to a helical shape because the radial confinement provided by the rigid formation boundary suppresses further lateral displacement of the casing. As the temperature is increased to the maximum value (275°C), helical buckling and the resulting local casing curvature continue to increase along with steam relaxation during the hold phase. When the casing cools, the curvature decreases as the compressive loads decrease, and with continued cooling, the casing passes from compression into tension.

Figure 8 presents the results of casing strain and curvature as a function of the radial cement voidage (i.e. where 0% voidage represents no voidage and fully supported casing, while 100% voidage represents full voidage or no cement in casing-formation annulus). As shown in Figure 8, the casing has 0.35% thermal strain and zero curvature if it is fully supported by cement. This total thermal strain of 0.35% consists of 0.26% elastic strain and 0.09% plastic strain, as shown in Figure 4. If there is a region where there is no cement (i.e. 100% voidage), casing buckling can result in 1.45% total casing strain and 138º/30 m local casing curvature. With this degree of

curvature, it may not be possible to install equipment or access the wellbore below this region of the well. Also, the high plastic strain could result in casing failure (e.g. at a connection). This example demonstrates that casing buckling can cause serious concerns for casing structural integrity and well serviceability, and it illustrates the importance of ensuring that there is good cement placement in thermal wells.

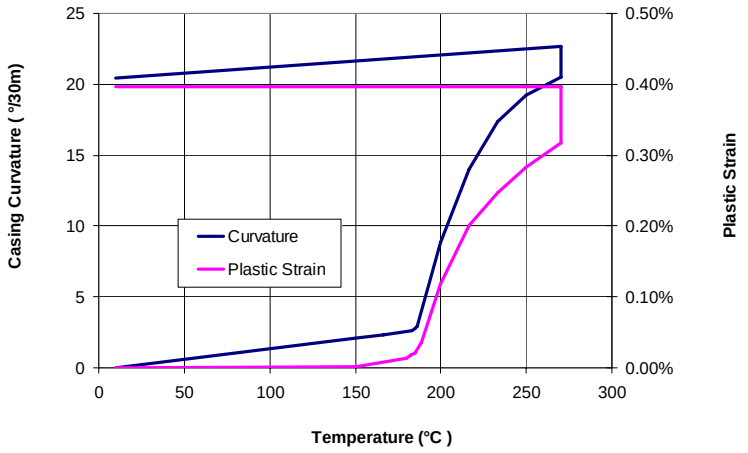

Figure 7. Casing curvature and plastic strain vs. temperature for casing under buckling.

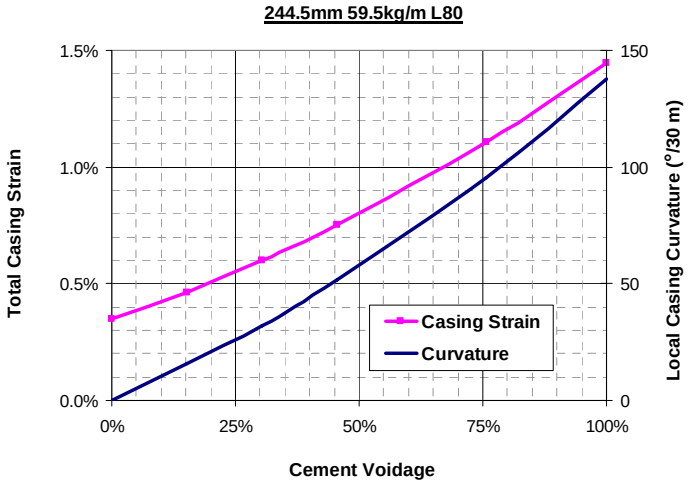

Figure 8. Casing strain and curvature vs. cement void at the end of the hold phase.

5. Analysis of Casing under Formation Shear Movement

5.1 Description of Loads

As evident from field experience in Canada and elsewhere, thermal wells are at risk of being exposed to formation movements such as those associated with non-uniform thermal expansion and contraction of various formation layers and reservoir pressure effects during operation. The relative lateral shifting of formation layers often occurs at a thin layer at a particular depth interval. This shift can cause severe shear loading of the casing strings that penetrate these intervals. In many cases, because the zone is thin, the resulting shear displacement occurs over a very short interval, which causes high curvatures and corresponding large strains in the casing.

5.2 Analysis Models

Figure 9 shows a schematic representation of the finite element model used for the analysis of casing deformation under formation shear movement. The casing was modeled using axisymmetric solid elements that accommodate large, non-linear, asymmetric displacements. For this example and to simplify the analysis, the initial casing curvature was not considered in the formation shear loading analysis. This is reasonable since the formation shear movement results in very large local casing curvature; therefore, ignoring the initial wellbore curvature has little impact on the analysis results. The formations were modeled using formation spring elements, with one end of each formation spring element attached to the casing system and the other end attached to a global node at which the shear displacement was imposed.

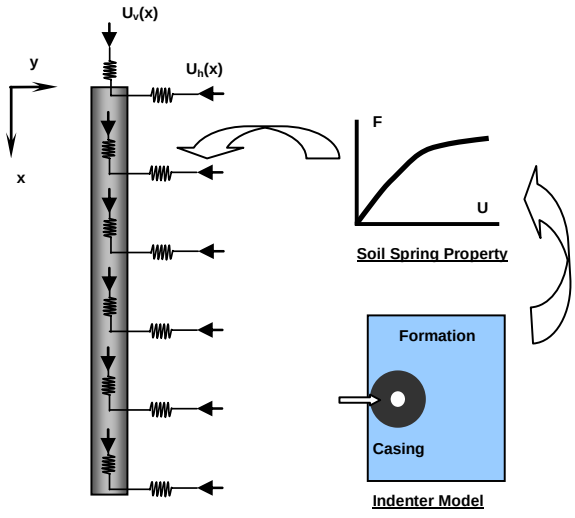

Figure 9. Schematic representation of finite element model for analyzing casing under formation shear movement.

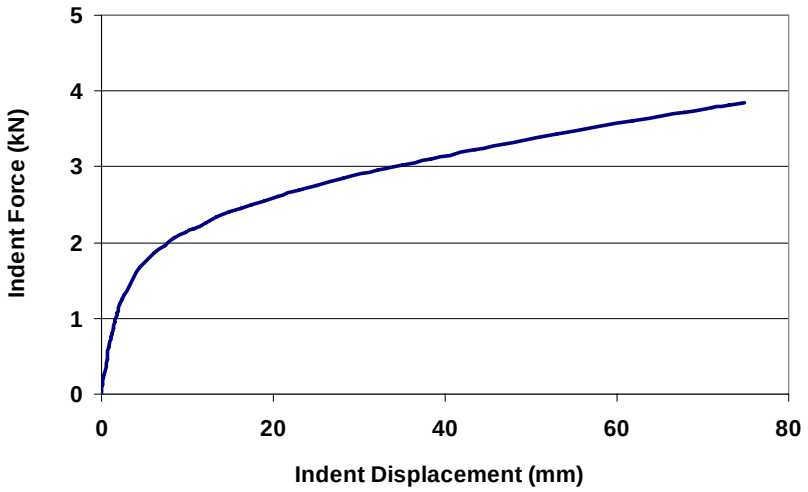

Figure 10. Indenter curve for 244.5 mm casing into the McMurray formation.

The stiffness and strength of the formation springs were determined using indenter curves generated by a finite element analysis of a rigid casing indenting into the formation, as shown in Figure 9. The indenting model consisted of a two-dimensional, plane-strain slice of formation material in the horizontal plane with a borehole in the center and a rigid indenter to represent the cement and casing. The indenter was moved laterally to impinge on the borehole wall and penetrate the formation. The Abaqus slide-line contact elements were used to model the interaction between the formation and indenter.

Figure 10 presents a typical indenter curve for a 244.5 mm OD casing acting at a 380 m depth in the McMurray formation (i.e. the typical production zone for SAGD wells in the Athabasca oil sands of Western Canada). The indenter curve appears to be initially linear to approximately 2 mm of formation displacement. However, as the formation yields, the force-displacement relationship becomes non-linear and the load-carrying capacity of the formation reduces as displacement is increased.

5.3 Analysis Example

This design example considers a 244.5 mm, 59.5 kg/m L80 casing under 30 mm formation shear displacement, which is consistent with the displacement observed in several field cases. It is also assumed that the formation shear movement occurs after heating the casing to 275ºC, also a reasonable scenario. The shear plane is assumed to be located at the mid-height of the casing model and the shear displacements are applied to the soil-end nodes of the soil spring elements in opposite directions over the two adjacent zones (i.e. relative to the shear plane).

Figure 11 presents the calculated lateral displacement and curvature along the casing within the shear interval resulting from the imposed formation shear movement. Note the lateral casing deformation is concentrated within the shear interval, with the deformation extending only about

0.5 m axially in either direction from the shear plane. The peak casing curvature of 250°/30 m occurs just below and above the shear plane. A plastic strain contour plot from a three-dimensional solid element model is also shown in Figure 11. As shown, the two peak curvature locations correspond to areas with the maximum plastic strain. The maximum plastic strain in this case was 1.8%, resulting from the combined effects of thermal cycle loading and high local curvature from formation shear movement.

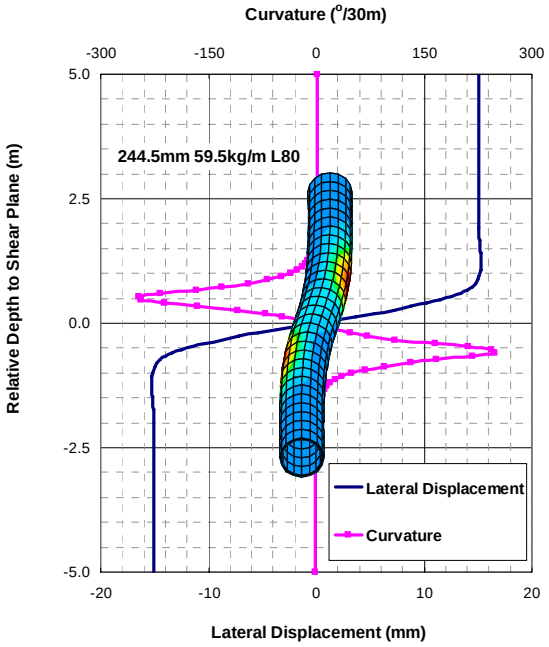

Figure 11. Casing lateral displacement and curvature caused by formation shear movement.

6. Conclusions

This paper presented numerical considerations in modeling casing deformation for thermally-operated wells. Three operation load scenarios were considered and modeled, including thermal cycle loading, casing buckling and formation shear movement. Results from analyses such as those described in this paper are often used by thermal operators to develop a sound basis for a plastic strain-based design of thermal well casings.

It was noted that the limitation of constitutive modeling of cyclic plasticity and creep strains with many of the commercial finite element programs is the key concern for thermal well designers in assessing the casing response through multiple thermal cycles. As a result of this limitation, the current suggested approach is to assess thermal casing behavior based on analyses of casing

material response under monotonic or single cycle load conditions. Further work is needed in developing a more reliable constitutive model for cyclic plasticity scenarios. This work will include developing cyclic plasticity theory and formulations, implementing the corresponding constitutive model into programs, and developing a cumulative damage criterion for assessing casing material damage through multiple thermal cycles.

7. Acknowledgement

The work was supported by C-FER Technologies, Canada. Technical review by Mr. T. Zahacy of C-FER Technologies is greatly appreciated.

8. References

1. CNRL Report, Wolf Lake and Primrose Expansion. Volume 1. Project Description. October 2000.
2. Ellyin, F., Xia, Z. and Wu, J., A New Elasto-Plastic Constitutive Model Inserted Into the User-Supplied Material Model of ADINA, Computers and Structures, Vol. 56, No. 2/3, pp.283-294, 1995.
3. Fu, Y., Yang, P., Han. G., and Hao, Z., Research of Casing Damage Mechanism and Prevention Measures for Thermal Production Wells of Heavy Oil, First World Heavy Oil Conference, Beijing, China, November 2006. Paper Number WHOC-2006-655.
4. Humphreys, K. J., Solanki, S.C. and Link, R.A, Qualification of Grade-55 Casing for Thermal Recovery Service; C-FER Final Report for Joint Industry Members, C-FER Project 88-14, 1991.
5. IOL Report, Application for Approval of Cold Lake Expansion Project. Section 4, Volume 1. February 1977.
6. Kaiser, T., Yung, V., and Bacon, R., Cyclic Mechanical and Fatigue Properties for OCTG Materials, SPE/PS-CIM/CHOA 97775, 2005 SPE Thermal Operations and Heavy Oil Symposium, Calgary, Alberta, Canada, 1-3 November, 2005.
7. Mroz, Z., On the Description of Anisotropic Work Hardening, Journal of Mech. Phys. Solids, 15 (1967), pp.163-175.
8. Xia, Z., and Ellyin, F., A Constitutive Model with Capacity to Simulate Complex Multiaxial Ratcheting Behaviour of Materials, International Journal of Plasticity, Vol. 13, No. 1/2. pp.127-142, 1997.
9. Xie, J., Understanding the Mechanisms of Well Casing Deformations; C-FER Final Report to Joint Industry Members, C-FER Project 99023, 2000.
10. XIE, J. Casing Design for Heavy Oil Wells. First World Heavy Oil Conference, Beijing, China, November 2006. Paper Number WHOC-2006-415.